Supporting Information for

"Subduction Beneath Laurentia Modified the Eastern North American Cratonic Edge: Evidence from P- and S-wave Tomography"

A. Boyce[1], I. D. Bastow[1], F. A. Darbyshire[2], A. G. Ellwood[1], A. Gilligan[1], V. Levin[3], and W. Menke[4]

[1]Department of Earth Science and Engineering, South Kensington Campus, Imperial College London, SW7 2AZ, UK.

[2]Centre de Recherche GEOTOP, Université du Québec à Montréal, Montréal, Québec, Canada.

[3]Department of Earth and Planetary Sciences, Rutgers University, Piscataway, NJ, USA.

[4]Lamont-Doherty Earth Observatory of Columbia University, Palisades, NY, USA.

Contents

Additional Supporting Information (Files uploaded separately)

1. Captions for large Tables S3, S4 (uploaded as separate Excel files).

1 Details of Figures S1 - S6

1.1 Figure S1

Figure S1 shows the checkerboard test for P-waves that indicates the short-wavelength resolving power of the model.

1.2 Figure S2

Figure S2 shows the checkerboard test for S-waves that indicates the short-wavelength resolving power of the model.

Corresponding author: Alistair Boyce, alistair.boyce10@imperial.ac.uk

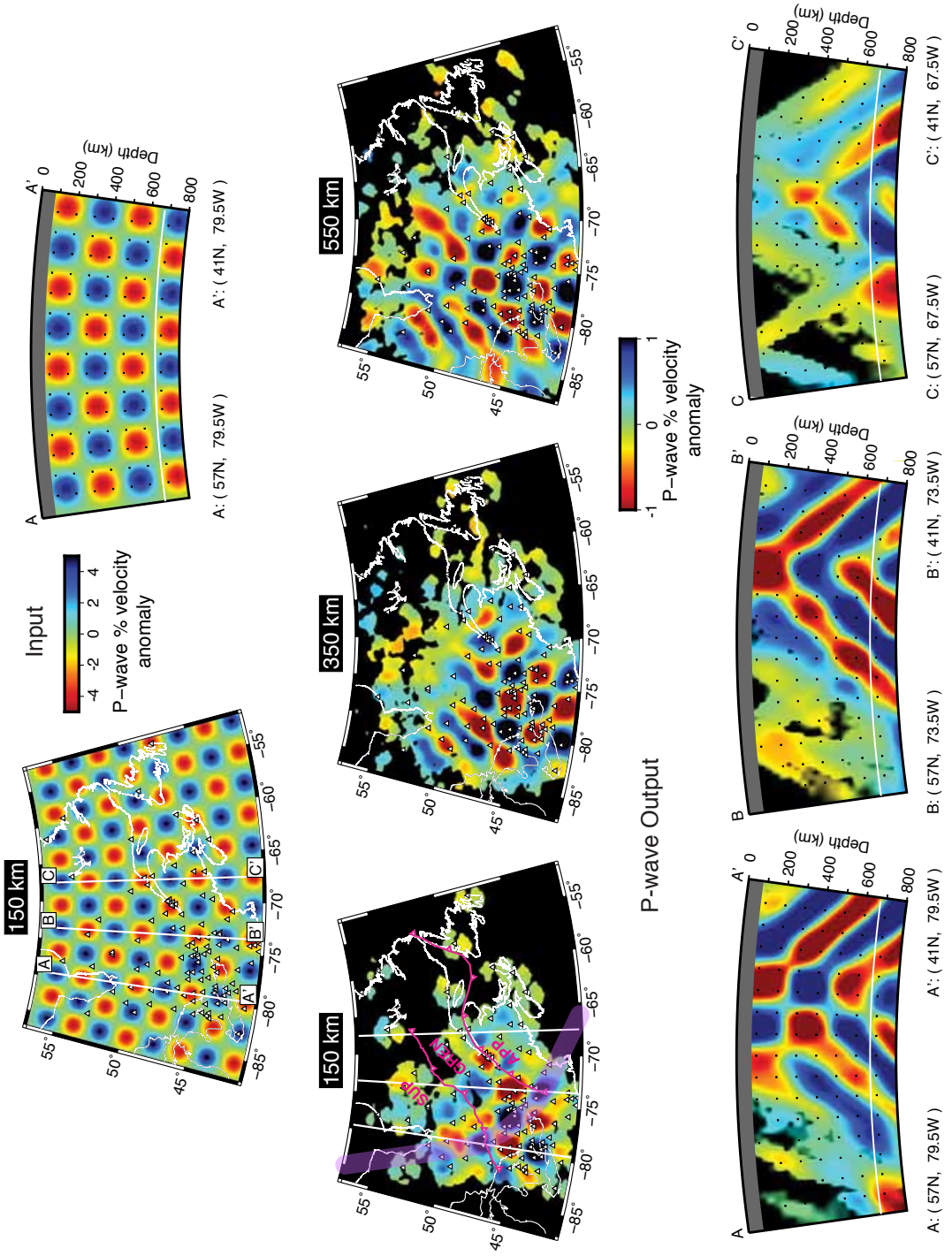

Figure 1. P-wave checkerboard resolution tests with 75 km wide input anomalies of $\delta V_P = \pm 5\%$ defined by Gaussian functions across their widths, placed at 150 km, 350 km, 500 km, 750 km, 950 km depths. Also shown are station locations (white triangles), tectonics (magenta lines) and the GMH track (lilac band). Regions with low (<3) ray hits and the top 75 km in cross-section are muted due to a lack of crossing rays and poor resolution.

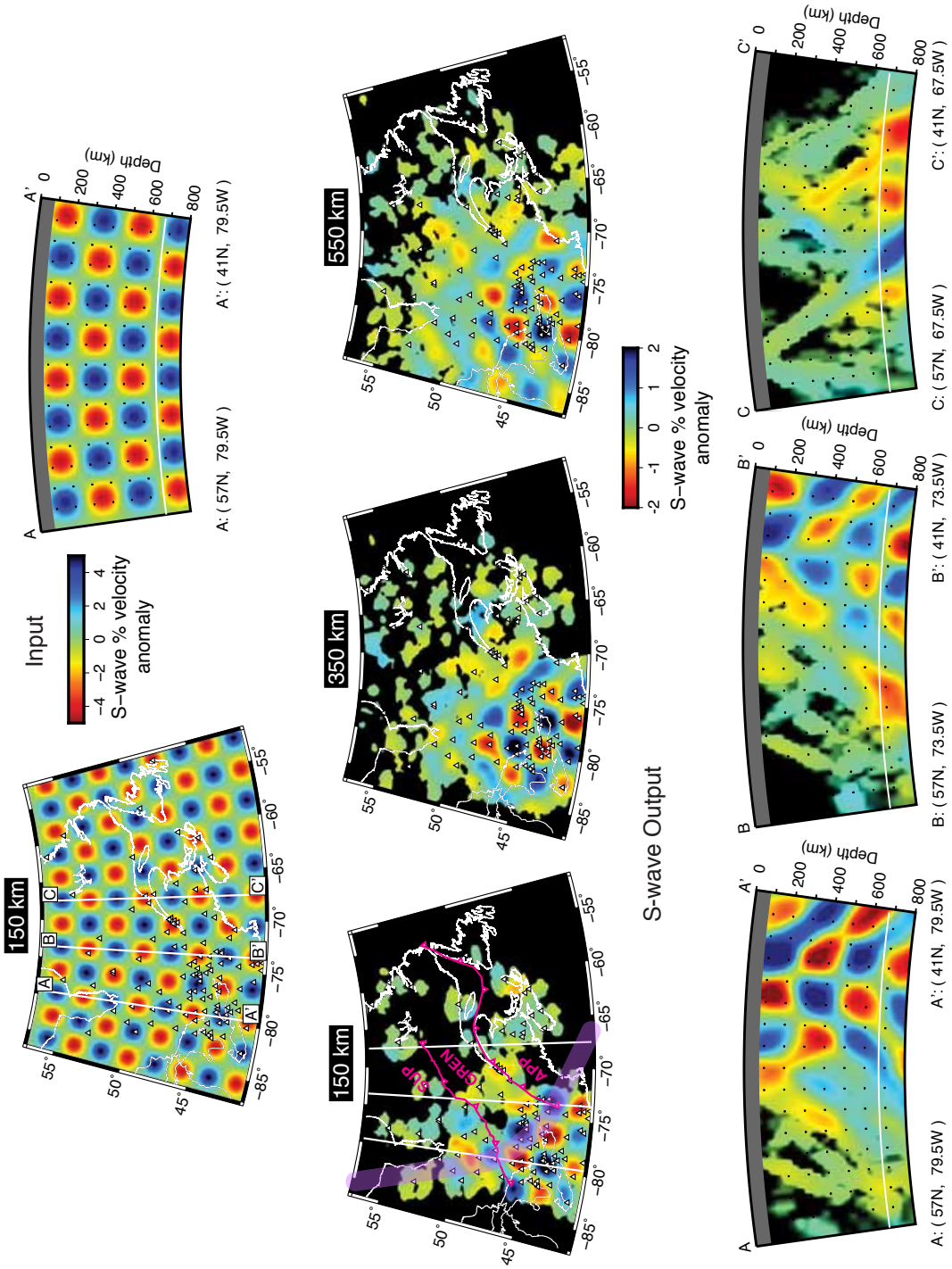

Figure 2. S-wave checkerboard resolution tests with 75 km wide input anomalies of $\delta V_S = \pm 5\%$ defined by Gaussian functions across their widths, placed at 150 km, 350 km, 500 km, 750 km, 950 km depths. Also shown are station locations (white triangles), tectonics (magenta lines) and the GMH track (lilac band). Regions with low (<3) ray hits and the top 75 km in cross-section are muted due to a lack of crossing rays and poor resolution.

1.3 Figure S3

This figure aims to show that if 'tectonic' structures are input with dipping interfaces the boundaries that are recovered also have dip (i.e. they are not vertical). Therefore features in the center of the model with vertical boundaries are assumed to be reliable. In the figure the P-wave model is used; the S-wave model produces similar results.

1.4 Figure S4

This figure shows the trade-off curve used to select the final P-wave model (F) from the non-unique inversion procedure. This accompanies the values in Table S1.

1.5 Figure S5

This figure shows the trade-off curve used to select the final S-wave model (E) from the non-unique inversion procedure. This accompanies the values in Table S2.

1.6 Figure S6

This figure displays the relative arrival-time residuals against backazimuth across both P- and S-wave datasets for selected stations in the Superior, Grenville and Appalachian terranes.

2 Details of Tables S1, S2

2.1 Table S1

This table shows the P-wave damping parameters (flattening and smoothing) that minimise primary and secondary spatial gradients in the model with the associated residual reduction. Models with heavy regularisation experience a decrease in residual reduction and vice-versa. Amplitude damping is not used in this inversion.

2.2 Table S2

This table shows the P-wave damping parameters (flattening and smoothing) that minimise primary and secondary spatial gradients in the model with the associated residual reduction. Models with heavy regularisation experience a decrease in residual reduction and vice-versa. Amplitude damping is not used in this inversion.

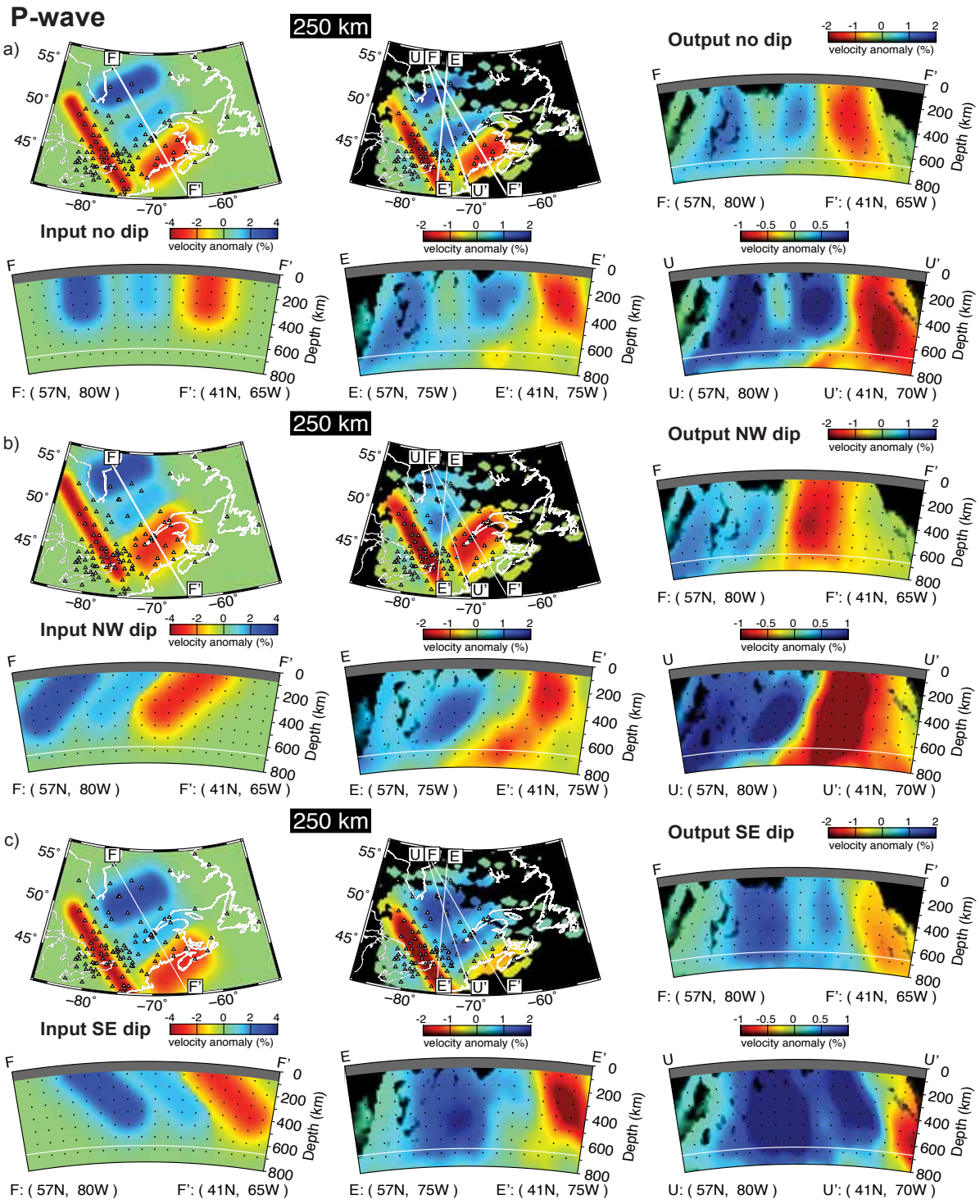

Figure 3. P-wave structural resolution test for dipping tectonic interfaces. Anomalies are defined as in the structural resolution testing in the main body of the paper but instead have 45° dip to the northwest (b) and southeast (c). Station locations are shown as white triangles. Regions with low (<3) ray hits and the top 75 km in cross-section are muted due to a lack of crossing rays and poor resolution.

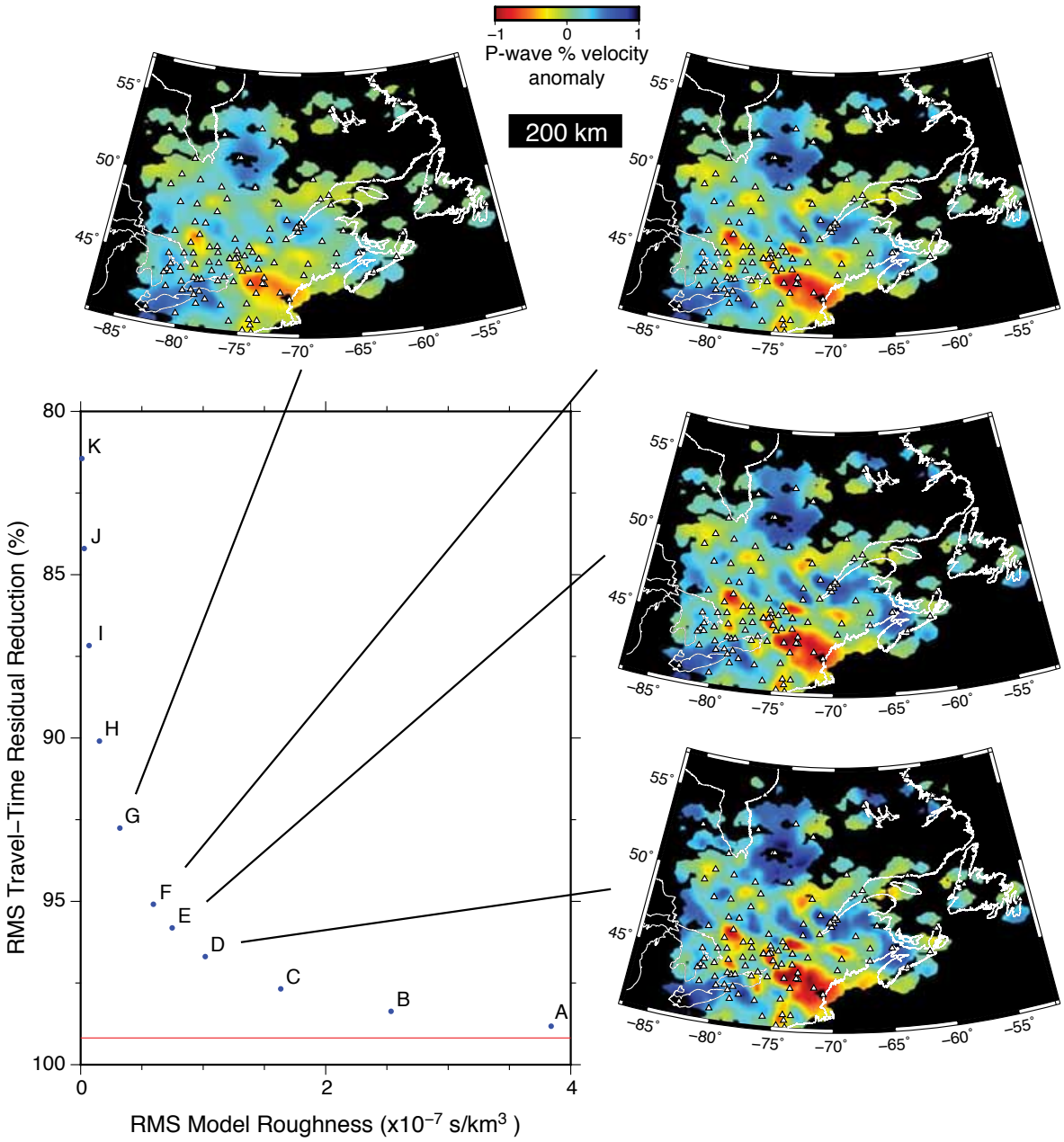

Figure 4. P-wave model Trade-off curve between model roughness and data fit. The corresponding weightings used in the inversions are given in Table S1. Depth slices taken at 200 km are subject to the same plotting conventions as for previous tomographic images. The red line is an MCCC derived estimate for data error, the ideal model sits above this line. Model F was picked in this case.

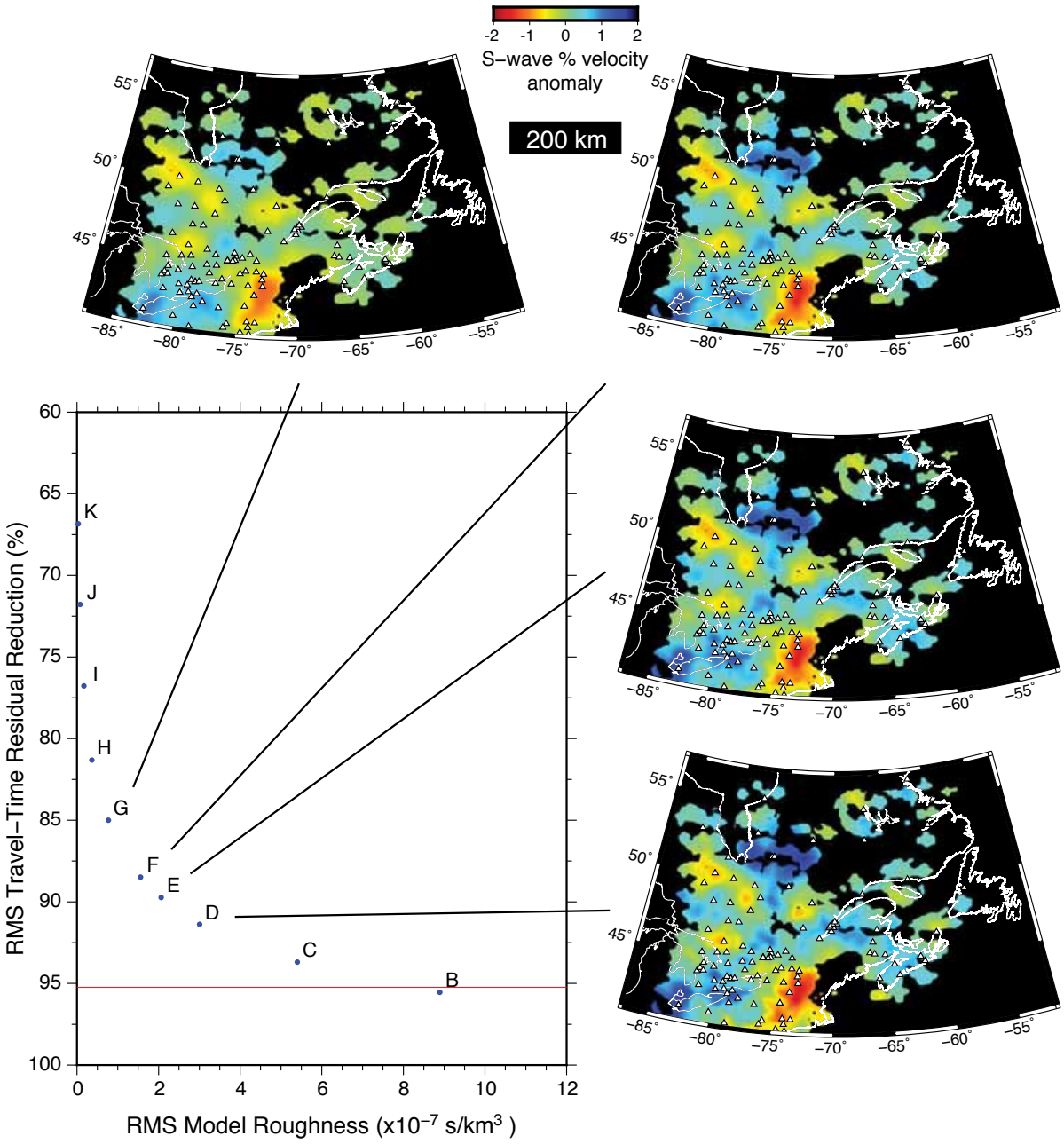

Figure 5. S-wave model Trade-off curve between model roughness and data fit. The corresponding weightings used in the inversions are given in Table S2. Depth slices taken at 200 km are subject to the same plotting conventions as for previous tomographic images. The red line is an MCCC derived estimate for data error, the ideal model sits above this line. Model E was picked in this case.

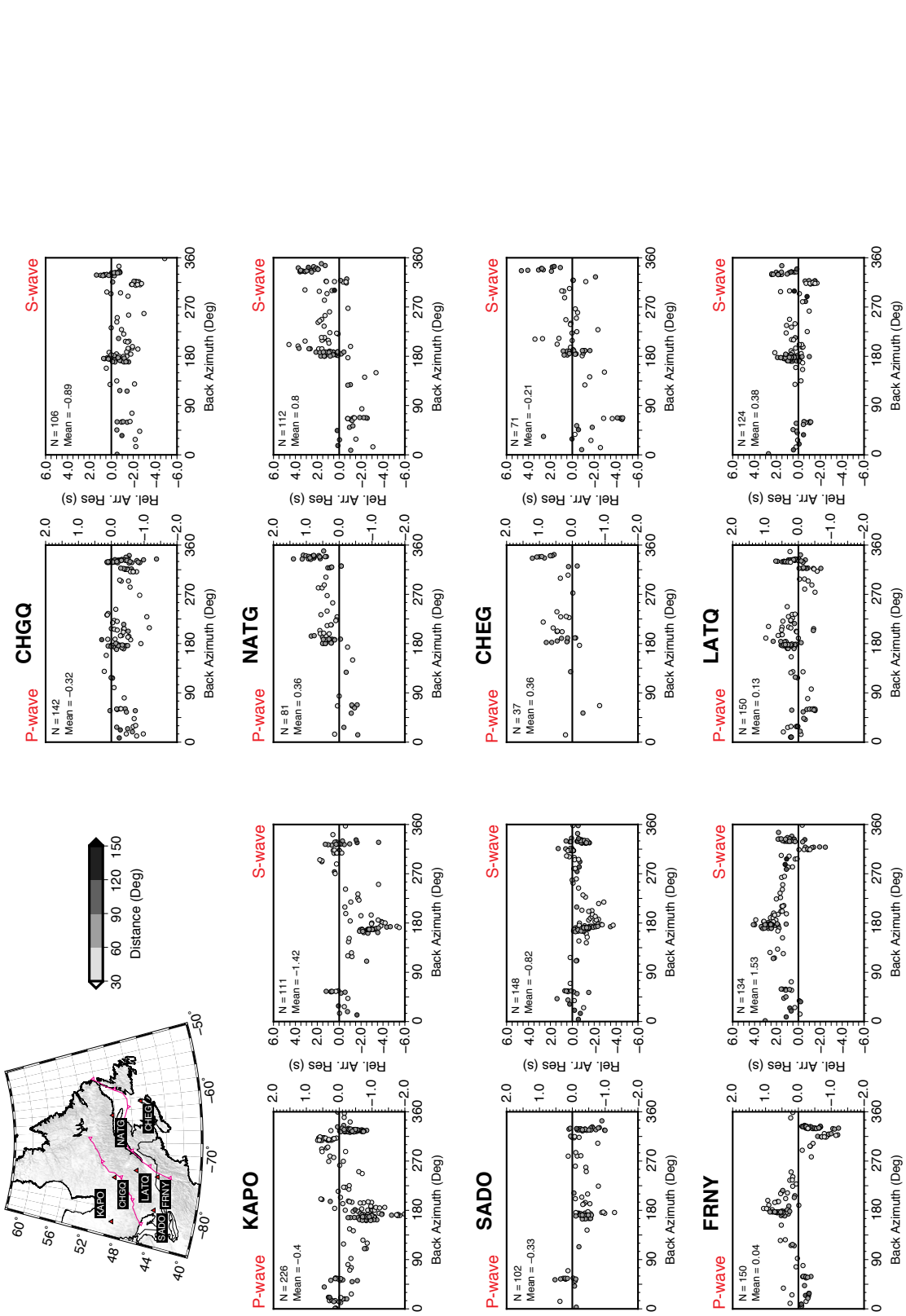

Figure 6. Comparison of relative arrival-time residuals against backazimuth for selected stations in the Superior, Grenville and Appalachian terranes for both P- and S-wave datasets. Station locations are shown on the inset map. Negative values are early arrivals (faster) and positive values are later arrivals (slower).

Table 1. P-wave Trade-off curve values

Inversion	Flattening	Smoothing	Residual Reduction
A	125	3750	98.8
B	250	7500	98.4
C	500	15000	97.7
D	1000	30000	96.7
E	1500	45000	95.8
F	2000	60000	95.1
G	4000	120000	92.8
H	8000	240000	90.1
I	16000	480000	87.2
J	32000	960000	84.2
K	64000	1920000	81.4

Table 2. S-wave Trade-off curve values

Inversion	Flattening	Smoothing	Residual Reduction
A	125	3750	96.9
B	250	7500	95.5
C	500	15000	93.7
D	1000	30000	91.4
E	1500	45000	89.7
F	2000	60000	88.5
G	4000	120000	85.0
H	8000	240000	81.3
I	16000	480000	76.8
J	32000	960000	71.8
K	64000	1920000	66.8

3 Dataset details

Also available is a 'JGR-manuscript-2016JB012838-data.tar.gz' file containing a README file, guide to VanDecar's code and P- and S-wave tomographic models and relative arrival-time residual datasets. Any further information can be obtained directly from AB (email: alistair.boyce10@imperial.ac.uk)

4 Additional Supporting Information

Outlined below is the description of the Excel table files uplaoded separately that contain the earthquake and station details used in the study.

4.1 Table S3

The table '2016JB012838-dt03.xlsx' gives details of all earthquakes used in the analysis.

Caption: Earthquakes used for this study - details and phases. Times are in 'YYYY-MM-DD HH:MM:SS' format.

4.1.1 Column 1

Date of Earthquake in YYYY-MM-DD format.

4.1.2 Column 2

Time of Earthquake in HH:MM:SS format.

4.1.3 Column 3

Latitude of Earthquake in Degrees.

4.1.4 Column 4

Longitude of Earthquake in Degrees.

4.1.5 Column 5

Depth of the Earthquake in kilometers.

4.1.6 Column 6

Backazimuth of Earthquake in Degrees from north.

4.1.7 Column 7

Great Circle Arc Distance of Earthquake in Degrees.

4.1.8 Column 8

Phases from the Earthquake used in the analysis.

4.2 Table S4

The table '2016JB012838-dt04.xlsx' gives details of all stations used in the analysis.

Caption: Location and details of seismic stations used in this study.

4.2.1 Column 1

Network Code

4.2.2 Column 2

Station Name.

4.2.3 Column 3

Latitude of Station in Degrees.

4.2.4 Column 4

Longitude of Station in Degrees.

4.2.5 Column 5

Elevation of the Station in kilometers.

4.2.6 Column 6

Instrument type: BB - Broadband instrument, SP - Short Period instrument.